Turkish Journal of Electrical Engineering & Computer Sciences

http://journals.tubitak.gov.tr/elektrik/

Research Article

Turk J Elec Eng & Comp Sci
(2017) 25: 1495 – 1507

doi:10.3906/elk-1503-207

Whole body motion control of humanoid robots using bilateral control

Emre SARIYILDIZ*, Hakan TEMELTAŞ
Department of Control and Automation Engineering, Faculty of Engineering, İstanbul Technical University, İstanbul, Turkey

Received: 24.03.2015 • **Accepted/Published Online:** 22.05.2016 • **Final Version:** 10.04.2017

Abstract: This paper deals with the whole body motion control problem of humanoid robots by using automatic and bilateral control methods. Advanced motion controllers are proposed so that human daily life activities, such as walking on an uneven terrain and contacting an unknown object, can be performed. It is shown that the uncertainty of environmental impedance variation is one of the main challenging issues in the design of the automatic control systems, i.e. a humanoid robot may easily lose its stability when it contacts an unstructured environment. A novel bilateral control method is proposed for humanoid robots so as to overcome the environmental uncertainty problem. It is shown that more dexterous and versatile tasks can be easily performed by transforming the skills of humans to humanoid robots in the proposed bilateral control system. A disturbance observer is used not only to achieve the robustness of the motion control system but also to perform sensorless contact motion control tasks. The performance of sensorless contact force estimation is significantly improved by deriving the exact dynamic model of humanoid robots. A floating point base exact dynamic model is derived by using the extended Newton–Euler algorithm. A new robot simulator is designed by using the proposed dynamic model and the Virtual Reality toolbox of MATLAB. Simulation results are given to show the validity of the proposals.

Key words: Bilateral control, bipedal locomotion, floating point base dynamics, simulator design, whole body control

1. Introduction

In the last four decades, humanoid robots have been extensively studied since they have several superiorities over other locomotion methods such as robots that use wheels and caterpillars [1–5]. For example, humanoid robots have significant capabilities to perform general tasks in human environments thanks to their mechanical structures so they can be used to assist human beings in several different applications [6–9]. However, current humanoid robots are still far from being a part of our daily life due to their insufficient performances [10,11].

Although more attention has been paid to lower body control, i.e. bipedal locomotion, upper body control is as important as lower body control when a humanoid robot performs a general task in a human environment [1,12–17]. For example, several tasks such as moving an object and assisting humans require not only locomotion but also interaction with upper limbs. Moreover, upper body control can be used to improve the balance and performance of bipedal locomotion. It is obvious that more dexterous and versatile tasks can be performed by considering whole body motion control of humanoid robots [18, 19]. However, it is a quite challenging task due to the highly nonlinear robot dynamics and redundant mechanical structure. The stability of the environmental interaction control is one of the most challenging issues due to large environmental

*Correspondence: esariyildiz@itu.edu.tr

uncertainties, e.g., the geometrical shape and impedance characteristics of an unstructured environment [20]. Recently, increased attention has been paid to whole body motion control of humanoid robots; however, the proposed solutions suffer from performance limitations and controller complexities [19,21,22].

In this paper, whole body motion control of a humanoid robot is carried out by using automatic and bilateral control methods. Advanced motion controllers are proposed to perform humans' daily life activities such as walking on an uneven terrain and interaction with an unknown object. It is shown that there are several challenging issues, such as trajectory generation for redundant mechanical structures and highly nonlinear dynamic models, to achieve the goal by using conventional automatic control methods. Moreover, the large uncertainty range of the unstructured environment may cause significant stability problems in contact motion control. A bilateral controller is proposed for humanoid robots so as to perform dexterous and versatile tasks by transforming humans' skills to robots. Not only the position but also the force information is transformed so as to mimic natural human motion. The main advantage of the proposed method is simplicity and practical efficiency. It can be implemented in many different application areas, such as rescue robotics and rehabilitation. A disturbance observer (DOb) is used to improve the robustness of the motion control system and achieve sensorless contact motion control. The performance of sensorless force estimation is significantly improved by deriving the floating point base exact dynamic model of humanoid robots. A new dynamic simulator is proposed by using the Virtual Reality toolbox of MATLAB and the derived exact dynamic model. It can be easily modified to improve the model of robots, e.g., a nonlinear friction model of servo systems can be easily considered. Simulation results are given to validate the proposal.

The rest of the paper is organized as follows. In Section 2, observer-based motion control systems and sensorless force estimation are briefly explained. In Section 3, whole body motion control systems are proposed by using automatic and bilateral control methods. In Sections 4 and 5, simulation results and a conclusion are given. The derivation of the floating point base exact dynamic model is given in the Appendix.

2. Disturbance observer-based motion controller design

To improve the robustness and estimate environmental impedance without using a force sensor, a DOb and reaction force observer (RFOb), which are shown in Figures 1a and 1b, respectively, are used in the design of the motion control systems [23]. In Figure 1, J_m and J_{mn} denote uncertain/exact and nominal inertias,

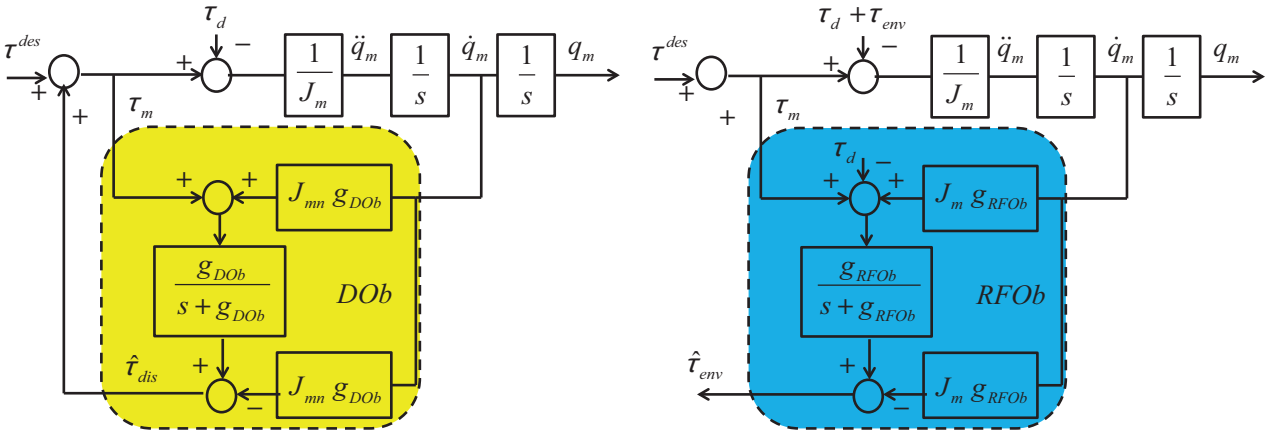

(a) A block diagram of a Dob

(b) A block diagram of an RFOb

Figure 1. Observer-based motion control systems.

respectively; τ_d and τ_{dis} denote external and total, which include external disturbances and plant uncertainties and disturbances, respectively; $\hat{\tau}_{dis}$ denotes the estimation of τ_{dis}; τ_{env} and $\hat{\tau}_{env}$ denote environmental force and its estimation, respectively; g_{DOb} and g_{RFOb} denote the bandwidths of the DOb and RFOb, respectively; and $q_m, \dot{q}_m$, and $\ddot{q}_m$ denote angle/position, velocity, and acceleration of the servo system, respectively.

A DOb estimates external disturbances and plant uncertainties such as external load, friction, and inertia variation. The robustness of the motion control systems is simply achieved by feeding back the estimated disturbances as shown in Figure 1a. It is directly related to the bandwidth of the DOb, i.e. the higher the bandwidth of the DOb is the more the robustness improves. However, it is limited by practical constraints such as noise and sampling frequency [23,24].

An RFOb is simply designed by subtracting system disturbances, such as friction, gravity, and Coriolis forces, from the input of a DOb as shown in Figure 1b. Since it is a model-based control method, deriving the exact dynamic model of the robot improves the performance of force estimation. Practical and theoretical superiorities of the RFOb over force sensors, such as expanding the bandwidth of force estimation, were proved by the authors in [20]. Sensorless force control is very important in humanoids since there may be many contact points in their practical implementations [25]. Several force sensors are required to detect/estimate contact forces; however, it significantly increases the cost. If an RFOb is used in motion control systems, then environmental impedance can be practically estimated without using a force sensor. Although joint space torques are simply estimated by using an RFOb, contact points should be known to control the operational space forces.

3. Whole body motion control of a humanoid robot in unstructured environments

In this section, advanced automatic and bilateral controllers are designed so that a humanoid robot can perform more dexterous and versatile tasks in an unstructured environment. First, only lower body motion control is considered and a walking pattern is generated by using the zero moment point (ZMP) on uneven terrain [26]. After that the balance of dynamic walking is improved by considering the upper body dynamics, i.e. the yaw moment is suppressed by swinging robot arms in the sagittal plane [27]. Second, contact motion control, in which a humanoid robot starts to contact and pushes an unknown object, is considered. Although high-performance sensorless contact motion control is achieved by using an RFOb, the implementation suffers from large uncertainty of the unstructured environment. Finally, a bilateral control system, in which human skills can be used to perform more dexterous tasks, is proposed for humanoid robots [28].

3.1. Automatic control

Let us start by considering dynamic walking on an uneven terrain. The ZMP is a well-known dynamic balance index for pedal locomotion systems [16]. It can be derived by calculating the total moment at the robot's foot as follows:

$$\tau_{\mathbf{ZMP}} = \dot{\mathbf{L}}_{\mathbf{w}} + \sum_i m_i \left(\mathbf{p}_{\mathbf{CoM_i}} - \mathbf{p}_{\mathbf{ZMP}}\right) \times \left(\ddot{\mathbf{p}}_{\mathbf{CoM_i}} - \upsilon_{\mathbf{g}}\right) \quad , \tag{1}$$

where $\tau_{\mathbf{ZMP}}$ denotes total moment at point $\mathbf{p}_{\mathbf{ZMP}}$ and $\mathbf{L}_{\mathbf{w}}$ denotes the angular momentum about the CoM defined by $\mathbf{L}_{\mathbf{w}} = \sum_i m_i \left(\mathbf{p}_{\mathbf{CoM}_i} - \mathbf{p}_{\mathbf{CoM}}\right) \times \dot{\mathbf{p}}_{\mathbf{CoM}_i} + {}_i\mathbf{R}^i\mathbf{I}_{ii}\mathbf{R}^T\mathbf{w}_i$. Please see the Appendix for the dynamic model of the humanoid robot and the explanation of terms in Eq. (1).

The ZMP is the point at which roll and pitch moments of $\tau_{\mathbf{ZMP}}$ are zero and is derived from Eq. (1) as

follows:

$$ {}^{x}p_{ZMP}=\frac{M{}^{x}p_{CoM}\left({}^{z}\ddot{p}_{CoM}+g\right)-M\left({}^{z}p_{CoM}-{}^{z}p_{ZMP}\right){}^{x}\ddot{p}_{CoM}-{}^{y}\dot{L}_{w}}{M\left({}^{z}\ddot{p}_{CoM}+g\right)} \quad , \tag{2} $$

$$ {}^{y}p_{ZMP}=\frac{M{}^{y}p_{CoM}\left({}^{z}\ddot{p}_{CoM}+g\right)-M\left({}^{z}p_{CoM}-{}^{z}p_{ZMP}\right){}^{y}\ddot{p}_{CoM}+{}^{x}\dot{L}_{w}}{M\left({}^{z}\ddot{p}_{CoM}+g\right)} \quad . \tag{3} $$

Eqs. (2) and (3) can be analytically solved if angular momentums are neglected and the CoM is kept fixed in a vertical direction, which are generally assumed in the implementations of bipedal locomotion. The trajectories of ${}^{x}p_{CoM}\left(t\right)$ are analytically derived as follows:

$$ \begin{aligned} {}^{x}p_{CoM}\left(t\right)&=\left({}^{x}p_{CoM}\left(t_0\right)-{}^{x}p_{ZMP}\right)\cosh\left(\omega\left(t-t_0\right)\right)+\frac{{}^{x}\dot{p}_{CoM}(t_0)}{\omega}\sinh\left(\omega\left(t-t_0\right)\right)+{}^{x}p_{ZMP}\\ {}^{x}\dot{p}_{CoM}\left(t\right)&=\omega\left({}^{x}p_{CoM}\left(t_0\right)-{}^{x}p_{ZMP}\right)\sinh\left(\omega\left(t-t_0\right)\right)+{}^{x}\dot{p}_{CoM}\left(t_0\right)\cosh\left(\omega\left(t-t_0\right)\right)\\ {}^{x}\ddot{p}_{CoM}\left(t\right)&=\omega^2\left({}^{x}p_{CoM}\left(t_0\right)-{}^{x}p_{ZMP}\right)\cosh\left(\omega\left(t-t_0\right)\right)+\omega{}^{x}\dot{p}_{CoM}\left(t_0\right)\sinh\left(\omega\left(t-t_0\right)\right) \end{aligned} \quad , \tag{4} $$

where $\omega=\sqrt{g/{}^{z}p_{CoM}}$. In Eq. (4), the initial position and velocities of the CoM are assigned by using [29].

Although the ZMP is generally used in flat terrains, it can be easily extended to an uneven terrain by using a virtual support polygon as shown in the Appendix [26]. If the ZMP is in the virtual support polygon, then dynamic walking can be achieved. The virtual support polygon is simply derived as follows:

$$ \begin{aligned} {}^{x}\hat{p}_i\left(t\right)&=\frac{{}^{x}p_i-{}^{x}p_{CoM}}{{}^{x}p_i-{}^{x}p_{CoM}}\left({}^{z}p_i-{}^{z}p_{CoM}\right)+x\\ {}^{y}\hat{p}_i\left(t\right)&=\frac{{}^{y}p_i-{}^{y}p_{CoM}}{{}^{y}p_i-{}^{y}p_{CoM}}\left({}^{z}p_i-{}^{z}p_{CoM}\right)+y \end{aligned} \quad , \tag{5} $$

where $\left({}^{x}p_i,{}^{y}p_i,{}^{z}p_i\right)$ and $\left({}^{x}\hat{p}_i,{}^{y}\hat{p}_i,{}^{z}\hat{p}_i\right)$ respectively denote the sole contact point and its projection on the virtual plane. Please see the Appendix for the definition of the virtual plane.

Although only horizontal moments are considered in the dynamic walking pattern generations, vertical moment, i.e. yaw moment, may also influence the balance. It can be suppressed by using upper body control, i.e. arm trajectories. It can be shown by using Eq. (1) as follows:

$$ \begin{aligned} {}^{z}\tau_{ZMP}&=\sum_i m_i\left({}^{x}p_{CoM_i}-{}^{x}p_{ZMP}\right){}^{y}\ddot{p}_{CoM_i}-\sum_i m_i\left({}^{y}p_{CoM_i}-{}^{y}p_{ZMP}\right){}^{x}\ddot{p}_{CoM_i}\\ &={}^{z}\hat{\tau}_{ZMP}+\sum_j m_j^{arm}\left({}^{x}p_{CoM_j}^{arm}-{}^{x}p_{ZMP}\right){}^{y}\ddot{p}_{CoM_j}^{arm}-\sum_j m_j^{arm}\left({}^{y}p_{CoM_j}^{arm}-{}^{y}p_{ZMP}\right){}^{x}\ddot{p}_{CoM_j}^{arm} \end{aligned} \quad , \tag{6} $$

where ${}^{z}\hat{\tau}_{ZMP}$ represents total yaw moment of a humanoid robot except robot arms. Eq. (6) directly shows that yaw moment can be suppressed by adjusting robot arms' trajectories. To suppress yaw moments, the sagittal plane trajectory, which is more natural than that of the frontal plane, is obtained as follows:

$$ {}^{x}\ddot{p}_{CoM_i}=\frac{{}^{z}\hat{\tau}_{ZMP}}{\sum_i m_i\left({}^{y}p_{CoM_i}-{}^{y}p_{ZMP}\right)_{arm}}. \tag{7} $$

To perform more dexterous tasks in an unstructured environment, contact motion of a humanoid robot's upper limbs should be considered. Compliance of the robot arms should be adequately adjusted to achieve safe and stable contact motions. Besides that, the ZMP pattern generation should be modified according to the acting

forces on robot arms to keep the balance of dynamic locomotion. Eq. (1) is modified when external forces act on robot arms as follows:

$$\tau_{\mathbf{ZMP}} = \dot{\mathbf{L}}_{\mathbf{w}} + \sum_i m_i \left(\mathbf{p}_{\mathbf{CoM_i}} - \mathbf{p}_{\mathbf{ZMP}}\right) \times \left(\ddot{\mathbf{p}}_{\mathbf{CoM_i}} - \upsilon_{\mathbf{g}}\right) + \sum_j \left(\mathbf{p}_j^{arm} - \mathbf{p}_{\mathbf{ZMP}}\right) \times \mathbf{f}_j^{arm}, \tag{8}$$

where $\mathbf{f}_j^{arm}$ denotes force acting on the robot arm at point $\mathbf{p}_j^{arm}$. The ZMP is similarly derived by setting ${}^x\tau_{ZMP} = {}^y\tau_{ZMP} = 0$ as follows:

$${}^x p_{ZMP} = \frac{M {}^x p_{CoM} \left({}^z\ddot{p}_{CoM} + g\right) - M \left({}^z p_{CoM} - {}^z p_{ZMP}\right) {}^x\ddot{p}_{CoM} - {}^y\dot{L}_w}{M \left({}^z\ddot{p}_{CoM} + g\right)} - \sum_j \frac{\left({}^z p_j^{arm} - {}^z p_{ZMP}\right)}{M \left({}^z\ddot{p}_{CoM} + g\right)} {}^x f_j^{arm}, \tag{9}$$

$${}^y p_{ZMP} = \frac{M {}^y p_{CoM} \left({}^z\ddot{p}_{CoM} + g\right) - M \left({}^z p_{CoM} - {}^z p_{ZMP}\right) {}^y\ddot{p}_{CoM} + {}^x\dot{L}_w}{M \left({}^z\ddot{p}_{CoM} + g\right)} - \sum_j \frac{\left({}^z p_j^{arm} - {}^z p_{ZMP}\right)}{M \left({}^z\ddot{p}_{CoM} + g\right)} {}^y f_j^{arm}. \tag{10}$$

Harada et al. proposed a new control method by considering Eqs. (2) and (3) and Eqs. (8)–(10) [30]. Pushing force is derived by considering the difference between the ZMP trajectories. Since not only feet but also robot hands come in contact with the environment, enhanced ZMP constraints should be considered to determine the ZMP support polygon as shown in [30]. Although ZMP trajectories can be modified to keep the balance, the stability of contact motion is still a very challenging problem due to the large uncertainty range of environmental impedance in practice [24].

3.2. Bilateral control

To perform humans' daily-life tasks in an unstructured environment, adaptability of humanoid robots should be improved. However, in reality, it is not an easy task to realize an autonomous humanoid robot that can safely work in an unstructured environment due to large uncertainties, such as environmental impedance. The ability of human adaptation to an unknown environment is one of the key points in achieving more dexterous robots. Humanoid robots can be easily adapted to unknown environments by using bilateral control since their dexterity and versatility can be improved by transforming humans' skills.

Four channel bilateral control (4chBC) is one of the most efficient bilateral control methods in the literature [28]. Control goals are defined in modal space, i.e. common and differential modes, as follows:

Common mode:

$$\mathbf{F_M} + \mathbf{F_S} = \mathbf{0}, \tag{11}$$

Differential mode:

$$\mathbf{X_M} - \mathbf{X_S} = \mathbf{0}, \tag{12}$$

where $\mathbf{X}_\bullet$ and $\mathbf{F}_\bullet$ represent the position and force of master and slave robots in joint or operational spaces, respectively.

Reproducibility and operationality are two important evaluation criteria in 4chBC systems. The former represents the fundamental goal of bilateral control, i.e. reproducing the slave side environment at the master side, and the latter represents how comfortably bilateral control operation is performed [28]. The ideal condition that satisfies perfect reproducibility and operationality is called transparency; however, it has limitations in practice [28,31].

The conventional 4chBC, in which joint space parameters are used in the design of modal space controllers, can be used when the same floating point base master and slave robots are used in the same environment. For example, two exoskeletons can be controlled by using conventional 4chBC in rehabilitation applications. However, it has some practical limitations in humanoid applications, e.g., if master and slave robots perform tasks in different environments, then conventional 4chBC cannot be directly implemented.

In this paper, a 4chBC system is designed by using operational space parameters instead of joint space ones so that the design flexibility of the master robot is improved. Besides that, automatic and bilateral control methods are simultaneously used in the lower and upper body control of a humanoid robot, respectively. A block diagram of the proposed bilateral control system is shown in Figure 2. In this figure, $\bullet_M$ and $\bullet_S$ denote master and slave, respectively; $\bullet^{OS}$ and $\bullet^{MS}$ denote operational and model spaces, respectively; $\mathbf{K_X}$, $\mathbf{K_{\dot{X}}}$, and $\mathbf{K_F}$ denote modal space position, velocity, and force control gains, respectively; $\mathbf{M}_n^{MS}$ denotes nominal inertia in modal space; FK and MST denote forward kinematics and modal space transformation, respectively; $MSDOb$ denotes the modal space disturbance observer; and $\mathbf{\Gamma}$ denotes the selection matrix of the modal space hybrid motion controller. The modal space transformation matrix is simply derived by considering the common and differential modes given in Eqs. (11) and (12). A DOb is designed in modal space so as to achieve decoupled hybrid motion control [32].

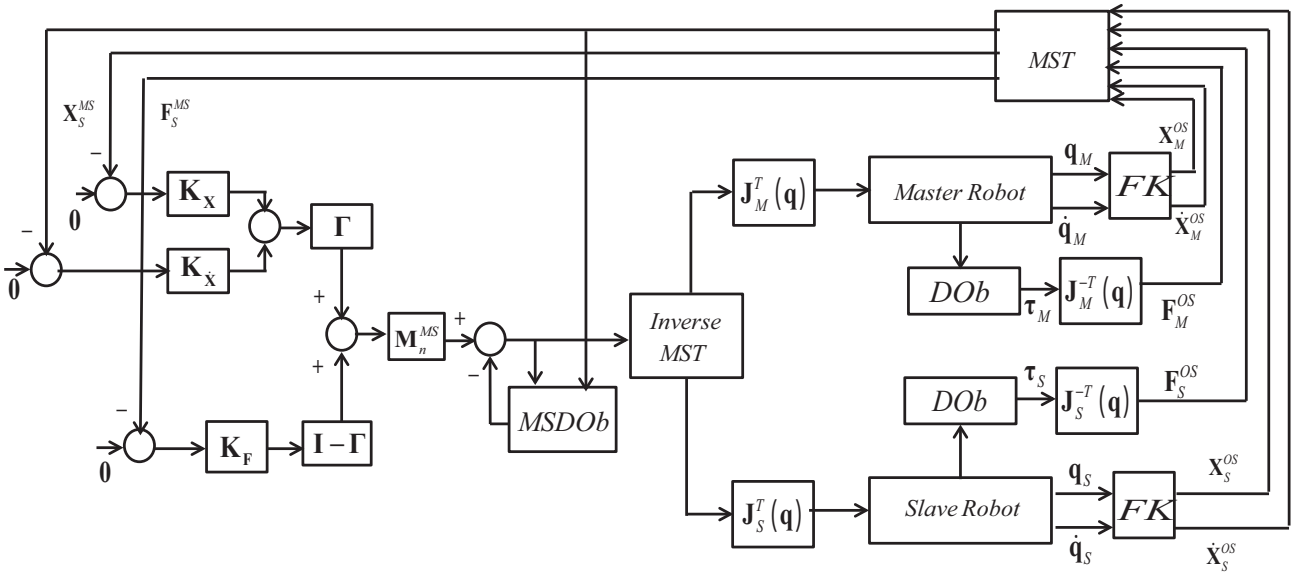

Figure 2. Modal space DOb-based bilateral control system.

4. Simulation results

In this section, whole body motion control simulations of a humanoid robot are presented. A new simulator is designed by using the exact dynamic model, which is derived in the Appendix, and the Virtual Reality toolbox of MATLAB. The simulations are conducted using an Intel Core i3 2.10 GHz processor, and the sampling rate of the simulations is 1 ms. In the simulations, free and contact motions are considered to perform dexterous tasks in an unstructured environment.

Let us start by considering the dynamic walking problem on uneven terrain as shown in Figures 3a and 3b. The virtual ZMP, which is proposed in Section 3, is used to generate the dynamic walking pattern on

uneven terrain. To suppress yaw moments, arm trajectories are generated by using Eq. (7). Figure 4 shows the CoM control results of the humanoid robot. It is clear from Figures 3 and 4 that the humanoid robot can walk on uneven terrain by using the virtual ZMP.

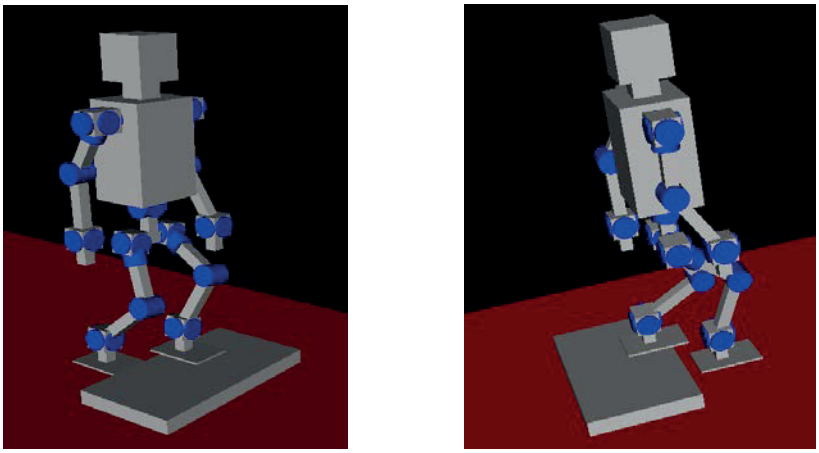

(a) t = 2.5 s. (b) t = 6.5 s.

Figure 3. Dynamic walking on an uneven terrain.

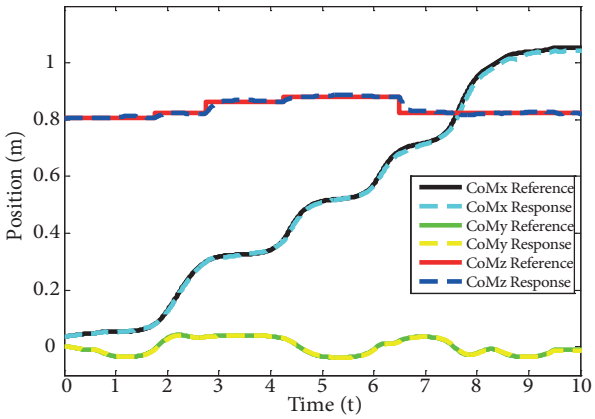

Figure 4. CoM of the humanoid robot when it walks on uneven terrain.

Let us now consider the free and contact motion control problems shown in Figures 5a and 5b, respectively. In Figure 5a, the humanoid robot waves its right hand when it walks on flat terrain. In this simulation, arm accelerations are kept small so that lower and upper body controllers are designed independently. Figures 6a and 6b show that the humanoid robot can follow the ZMP references when it conducts an upper body motion task. In Figure 5b, the humanoid robot contacts an unknown environment. For the sake of simplicity, position control is conducted in y and z directions and force control is conducted only in the x direction. Figures 7a and 7b respectively show the CoM of the humanoid robot in the vertical direction and force control results in the horizontal direction. Safe contact motion control is achieved by using low force control inputs and bandwidth, i.e. low force control gain, and the input is increased after contact occurs. In unsafe contact motion, relatively high force control input is used in a larger force control bandwidth. Figure 7 shows that the instability of contact motion directly influences the balance of the humanoid robot. It is obvious that the balance of the humanoid robot deteriorates as the environmental force is increased even if safe contact motion is achieved.

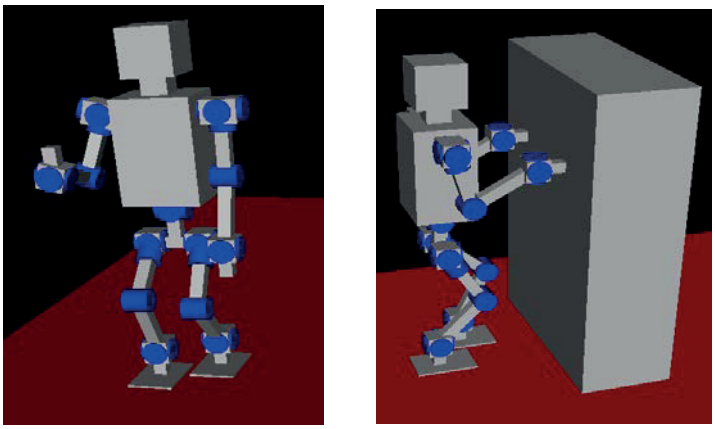

(a) Wave hand (b) Contact with an object

Figure 5. Free and contact motion control.

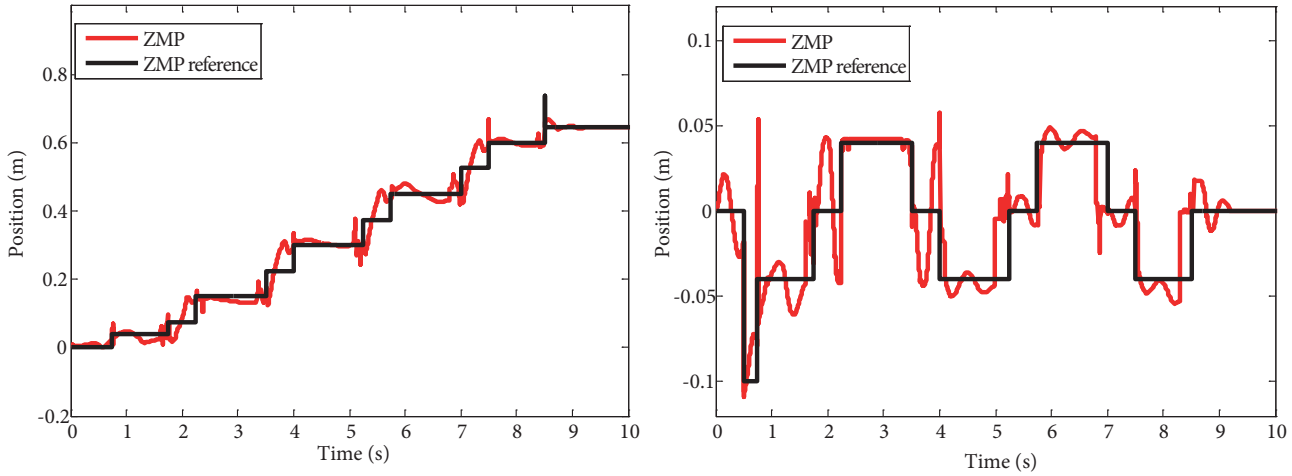

(a) ZMP in x direction (b) ZMP in y direction

Figure 6. ZMP control results of the robot in free motion.

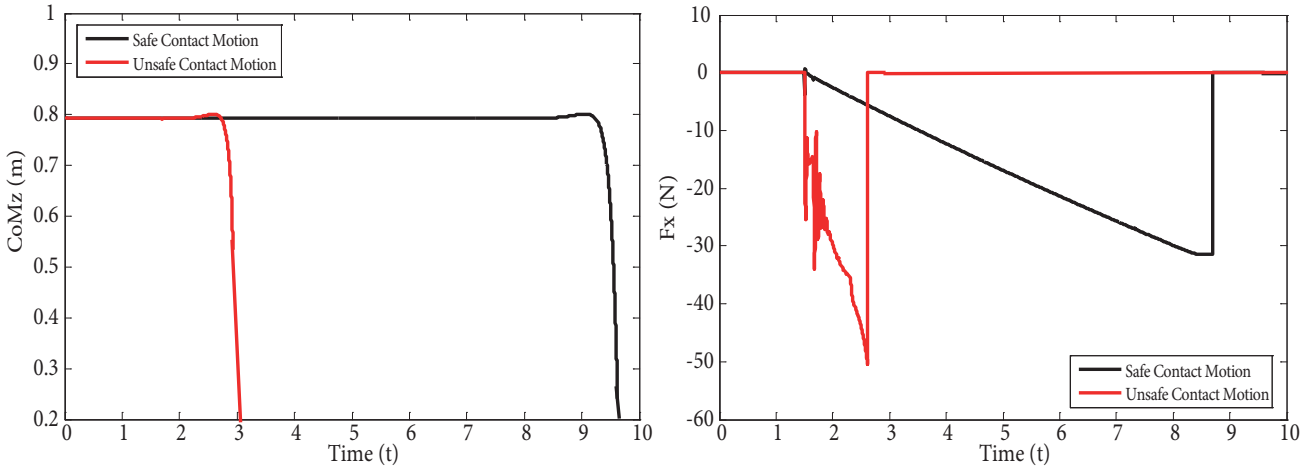

(a) Position of the CoM in vertical direction (z). (b) Applied force in horizontal direction (x).

Figure 7. CoM and force control responses of the robot in contact motion.

Let us now consider pushing motion as shown in Figure 8. The humanoid robot does not contact the environment initially and it starts walking towards the object that is unknown. To achieve safe contact motion, low force control input and gain are used as discussed before. After contact occurs, the force control input is increased to determine whether the object is movable or not. If it is movable, i.e. the humanoid robot can keep the balance when it applies force to move the object, then the humanoid robot can push the object as shown in Figures 8a and 8b. However, if the maximum applicable force of the humanoid robot, e.g., as shown in Figure 7b, is not sufficient to move the object, then the robot should stop increasing the force to keep the balance. The dynamic walking pattern is obtained by using Eqs. (8)–(10).

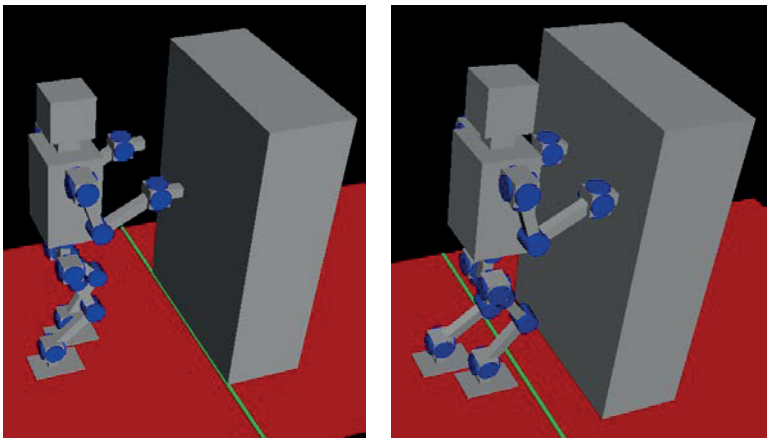

(a) t = 2.5 s. (b) t = 6.0 s.

Figure 8. Pushing an unknown object.

So far, the humanoid robot is controlled by generating upper and lower body trajectories. However, the trajectory generation is a complicated task due to the redundant structure. Moreover, the humanoid robot should adapt to the unknown environment to achieve safe contact motion; however, this is also a challenging task since open environments have very large uncertainties in general. Therefore, bilateral control, in which human skills can be used to improve the adaptability of humanoid robots, is used as shown in Figure 9. In Figure 9a, conventional 4chBC is implemented by using the same master and slave robots. It can be realized by using a wearable master robot, i.e. exoskeleton, which has the same structure as the humanoid robot's one. In Figure 9b, automatic control is used in the lower body of the humanoid robot; however, the upper body is controlled by using the proposed bilateral control system in which operational space parameters are used in the design of the modal space controller. The proposed bilateral control system is more practical than the conventional one and can be implemented by using several different master robot structures. Figures 10a and 10b respectively show that the position and force control goals are achieved, i.e. high reproducibility is obtained, in the operational space by using the proposed bilateral control system. Moreover, high operationality is achieved thanks to the high-performance sensorless force estimation.

5. Conclusion

In this paper, the whole body motion control problem of humanoid robots is considered to improve their dexterity and versatility. Advanced automatic and bilateral control systems are proposed so that humanoid robots can safely perform tasks in unstructured environments. It is shown that the large uncertainty range of the unstructured environment is one of the most challenging problems when automatic control methods are used

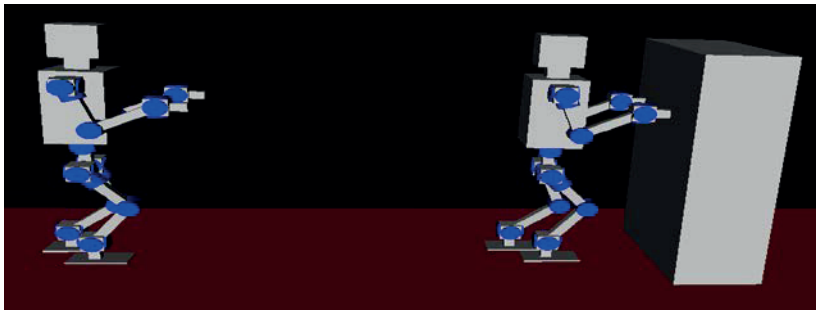

(a) Modal space transformation w.r.t. joint space parameters.

(b) Modal space transformation w.r.t. operational space parameters.

Figure 9. Bilateral control applications.

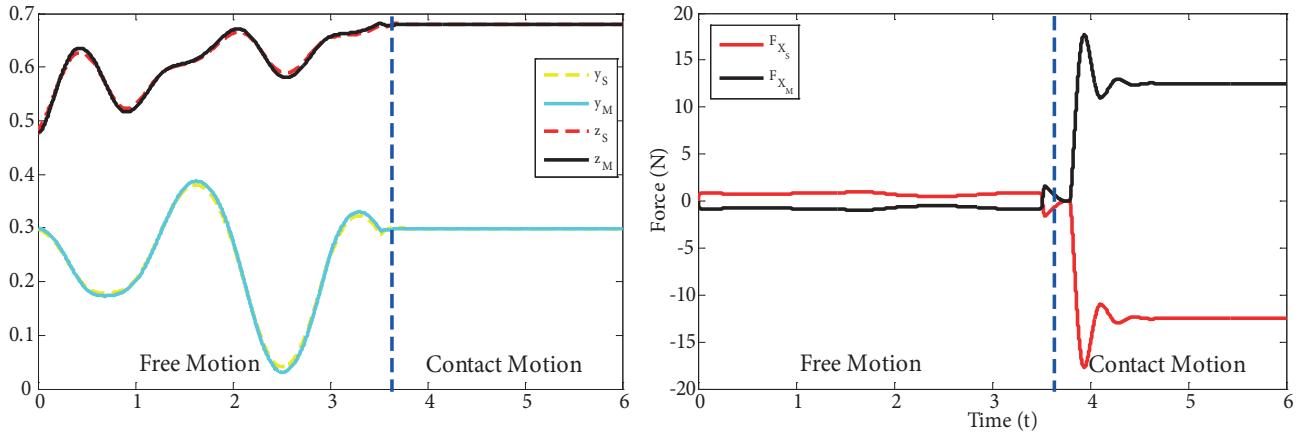

(a) Position responses of master and slave robots.

(b) Force responses of master and slave robots

Figure 10. Bilateral control responses (right arm).

in practice. However, robots can safely perform tasks in unstructured environments by using the adaptation skills of humans when bilateral control is used. Two different bilateral controllers are proposed to achieve more flexibility in the design of master robots. A DOb-based motion controller is used not only to improve the robustness but also estimate contact forces without using a force sensor. It is very practical in humanoid applications since there may be several contact points when robots perform tasks in unstructured environments. The performance of sensorless force estimation is significantly improved by deriving the floating point base exact dynamic model of humanoid robots. A new simulator is designed using the dynamic model and the Virtual Reality toolbox of MATLAB. Simulation results are given to verify the proposals.

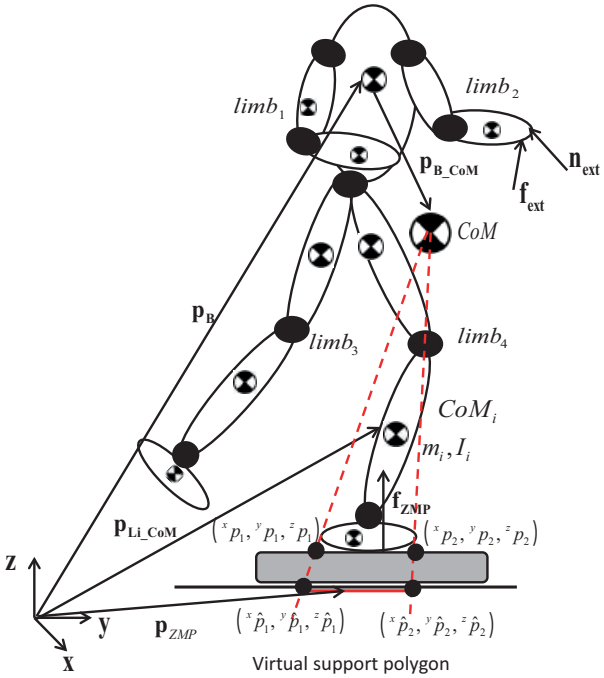

Figure 11. A general structure for a humanoid robot.

References

[1] Takanishi A, Tochizawa M, Takeya T, Karaki H, Y, Kato I. Realization of dynamic biped walking stabilized with trunk motion under known external force. In: 1989 4th Advanced Robotics Conference; 13–15 June 1989; Columbus, OH, USA. Berlin, Germany: Springer-Verlag. pp. 299-311.

[2] Sakagami Y, Watanabe R, Aoyama C, Matsunaga S, Higaki N, Fujimura K. The intelligent ASIMO: system overview and integration. In: IEEE 2002 Intelligent Robots and Systems Conference; 30 September–4 October 2002; Lausanne, Switzerland. New York, NY, USA: IEEE. pp. 2478-2483.

[3] Stiefelhagen R, Ekenel HK, Fugen C, Gieselmann P, Holzapfel H, Kraft F, Nickel K, Voit M, Waibel A. Enabling multimodal human–robot interaction for the Karlsruhe humanoid robot. IEEE T Robot 2007; 23: 840-851.

[4] Yongwook C, Jaeseung J, Sungho J. Toward brain-actuated humanoid robots: asynchronous direct control using an EEG-gased BCI. IEEE T Robot 2012; 28: 1131-1144.

[5] Kim K, Cha YS, Park JM, Lee JY, You BJ. Providing services using network-based humanoids in a home environment. IEEE T Consum Electr 2011; 57: 1628-1636.

[6] Shafii N, Reis LP, Rossetti RJF. Two humanoid simulators: comparison and synthesis. In: 2011 6th Iberian Information Systems and Technologies Conference; 15–18 June 2011; Chaves, Portugal.

[7] Kemp CC, Fitzpatrick P, Hirukawa H, Yokoi K, Harada K, Matsumoto Y. Humanoids. In: Sciliano B, Khatib O, editors. Handbook of Robotics. Berlin, Germany: Springer-Verlag, 2008. pp. 1307-1335.

[8] Kaneko K. Towards emergency response humanoid robots. In: 2012 9th France-Japan and 7th Europe-Asia Mechatronics Congress, Research, and Education; 21–23 November 2012; Paris, France.

[9] Levi N, Kovelman G, Geynis A, Sintov A, Shapiro A. The DARPA virtual robotics challenge experience. In: IEEE 2013 Safety, Security, and Rescue Robotics Symposium; 21–26 October 2013; Linkoping, Sweden. New York, NY, USA: IEEE. pp. 1-6.

[10] Durán B, Thill S. Rob's robot: current and future challenges for humanoid robots. In: Zaier R, editor. The Future of Humanoid Robots - Research and Applications. Rijeka, Croatia: InTech, 2012. pp. 279-300.

[11] Ohashi E, Aiko T, Tsuji T, Nishi H, Ohnishi K. Collision avoidance method of humanoid robot with arm force. IEEE T Ind Electron 2007; 54: 1632-1641.

[12] Khosravi B, Yurkovich S, Hemami H. Control of a four-link biped in a back somersault maneuver. IEEE T Syst Man Cyb 1987; 17: 303-311.

[13] Hernaández-Santos C, Rodriguez-Leal E, Soto R, Gordillo JL. Kinematics and dynamics of a new 16 DOF humanoid biped robot with active toe joint. Int J Adv Robot Syst 2012; 9: 190-202.

[14] Fujimoto Y, Kawamura A. Simulation of an autonomous biped walking robot including environmental force interaction. IEEE Robot Autom Mag 1998; 5: 33-42.

[15] Kajita S, Espiau B. Legged robots. In: Sciliano B, Khatib O, editors. Handbook of Robotics. Berlin, Germany: Springer-Verlag, 2008. pp. 361-390.

[16] Kajita S, Tani K. Study of dynamic biped locomotion on rugged terrain-derivation and application of the linear inverted pendulum mode. In: IEEE 1991 Robotics and Automation Conference; 9–11 April 1991; Sacramento, CA, USA. New York, NY, USA: IEEE. pp. 1405-1411.

[17] Motoi N, Ikebe M, Ohnishi K. Real-time gait planning for pushing motion of humanoid robot. IEEE T Ind Inform 2007; 3: 154-163.

[18] Yoshikawa T, Khatib O. Compliant motion control for a humanoid robot in contact with the environment and humans. In: IEEE 2008 Intelligent Robots and Systems Conference; 22–26 September 2008; Nice, France. New York, NY, USA: IEEE. pp. 211-218.

[19] Sentis L, Khatib O. Synthesis of whole-body behaviors through hierarchical control of behavioral primitives. Int J Hum Robot 2005; 4: 505-518.

[20] Sariyildiz E, Ohnishi K. On the explicit robust force control via disturbance observer. IEEE T Ind Electron 2015; 62: 1581-1589.

[21] Fok CL, Johnson G, Yamokoski JD, Mok A, Sentis L. Controlit! - a middleware for whole-body operational space control. Int J Hum Robot 2016; 13: 550040.

[22] Moro FL, Gienger M, Goswami A, Tsagarakis NG, Caldwell DG. An attractor-based whole-body motion control (WBMC) system for humanoid robots. In: IEEE 2013 Humanoid Robots Conference; 15–17 October 2013; Atlanta, GA, USA. New York, NY, USA: IEEE. pp. 42-49.

[23] Sariyildiz E, Ohnishi K. Stability and robustness of disturbance observer-based motion control systems. IEEE T Ind Electron 2015; 62: 414-422.

[24] Sariyildiz E, Ohnishi K. An adaptive reaction force observer design. IEEE-ASME T Mech 2015; 20: 750-760.

[25] Yoshikai T, Fukushima H, Hayashi M, Inaba M. Development of soft stretchable knit sensor for humanoids' whole-body tactile sensibility. In: IEEE 2009 Humanoid Robots Conference; 7–10 December 2009; Paris, France. New York, NY, USA: IEEE. pp. 624-631.

[26] Sato T, Sakaino S, Ohashi E, Ohnishi K. Walking trajectory planning on stairs using virtual slope for biped robots. IEEE T Ind Electron 2011; 58: 1385-1396.

[27] Zhang S, Huang Q, Wang H, Xu W, Ma G, Liu Y, Yu Z. The mechanism of yaw torque compensation in the human and motion design for humanoid robots. Int J Adv Robot Syst 2013; 10: 57-67.

[28] Iida W, Ohnishi K. Reproducibility and operationally in bilateral teleoperation. In: IEEE 2004 Advanced Motion Control Workshop; 25–28 March 2004; Kawasaki, Japan. New York, NY, USA: IEEE. pp. 217-222.

[29] Ugurlu B, Tsagarakis NG, Papastavridis E, Caldwell DG. Compliant joint modification and real-time dynamic walking implementation on bipedal robot cCub. In: IEEE 2011 International Conference on Mechatronics; 13–15 April 2011; İstanbul, Turkey. New York, NY, USA: IEEE. pp. 833-838.

[30] Harada K, Kajita S, Kaneko K, Hirukawa H. Pushing manipulation by humanoid considering two-kinds of ZMPs. In: IEEE 2003 Robotics and Automation Conference; 14–19 September 2003; Taipei, Taiwan. New York, NY, USA: IEEE. pp. 1627-1632.

[31] Lawrence D.A. Stability and transparency in bilateral teleoperation. IEEE T Robotic Autom 1993; 9: 624-637.

[32] Nozaki T, Mizoguchi T, Ohnishi K. Decoupling strategy for position and force control based on modal space disturbance observer. IEEE T Ind Electron 2014; 61: 1022-1032.

[33] Mistry M, Buchli J, Schaal S. Inverse dynamics control of floating base systems using orthogonal decomposition. In: IEEE 2010 Robotics and Automation Conference; 3–7 May 2010; Anchorage, AK. New York, NY, USA: IEEE. pp. 3406-3412.

[34] Craig J. Introduction to Robotics: Mechanics and Control. 2nd ed. Boston, MA, USA: Addison-Wesley Longman, 1989.

Appendix. Dynamic model of a humanoid robot

Figure 11 shows a general structure for a humanoid robot that has four limbs connected to a free floating base link [14,33]. The closed form dynamic model is derived as follows:

$$\left[\begin{array}{cc} {}^{\mathbf{B}}\mathbf{M}_{\mathbf{B}} & {}^{\mathbf{B}}\mathbf{M}_{\mathbf{L}} \\ {}^{\mathbf{L}}\mathbf{M}_{\mathbf{B}} & {}^{\mathbf{L}}\mathbf{M}_{\mathbf{L}} \end{array}\right] \underbrace{\left[\begin{array}{c} \ddot{\mathbf{x}}_{\mathbf{B}} \\ \ddot{\mathbf{x}}_{\mathbf{L}} \end{array}\right]}_{\ddot{\mathbf{x}}} + \left[\begin{array}{c} \mathbf{c}_{\mathbf{B}}\left(\mathbf{x},\dot{\mathbf{x}}\right) \\ \mathbf{c}_{\mathbf{L}}\left(\mathbf{x},\dot{\mathbf{x}}\right) \end{array}\right] + \left[\begin{array}{c} \mathbf{g}_{\mathbf{B}}\left(\mathbf{x}\right) \\ \mathbf{g}_{\mathbf{L}}\left(\mathbf{x}\right) \end{array}\right] = \left[\begin{array}{c} \mathbf{0} \\ \tau_{\mathbf{L}} \end{array}\right] + \mathbf{J}^{\mathbf{T}}\mathbf{F}, \tag{A.1}$$

where $\ddot{\mathbf{x}}_{\mathbf{B}} = \left[\begin{array}{cc} \dot{\mathbf{v}}^T & \dot{\mathbf{w}}^T \end{array}\right]^T$ denotes base-link accelerations in which $\dot{\mathbf{v}}$ and $\dot{\mathbf{w}}$ represent linear and angular acceleration vectors, respectively; ${}^{\mathbf{B}}\mathbf{M}_{\mathbf{B}} = \left[\begin{array}{cc} \mathbf{m}_{\dot{\mathbf{v}}\dot{\mathbf{v}}} & \mathbf{m}_{\dot{\mathbf{v}}\dot{\mathbf{w}}} \\ \mathbf{m}_{\dot{\mathbf{w}}\dot{\mathbf{v}}} & \mathbf{m}_{\dot{\mathbf{w}}\dot{\mathbf{w}}} \end{array}\right]$ denotes the inertia matrix of the base-link, in which $\mathbf{m}_{\dot{\mathbf{v}}\dot{\mathbf{v}}}$, $\mathbf{m}_{\dot{\mathbf{w}}\dot{\mathbf{w}}}$ and $\mathbf{m}_{\dot{\mathbf{v}}\dot{\mathbf{w}}}$ are the inertia submatrices related to the linear and angular accelerations, respectively; $\ddot{\mathbf{x}}_{\mathbf{L}}$ denotes the accelerations of limbs' joints; ${}^{\mathbf{L}}\mathbf{M}_{\mathbf{L}} = \left[\begin{array}{ccc} \mathbf{m}_{11} & \cdots & \mathbf{m}_{1n} \\ \vdots & \ldots & \vdots \\ \mathbf{m}_{n1} & \cdots & \mathbf{m}_{nn} \end{array}\right]$ denotes the limbs' inertia matrix, in which $\mathbf{m}_{ij}$ is the inertia submatrix related to the ith and jth limbs; ${}^{\mathbf{B}}\mathbf{M}_{\mathbf{L}} = {}^{\mathbf{L}}\mathbf{M}_{\mathbf{B}}^T = \left[\begin{array}{ccc} \mathbf{m}_{\dot{\mathbf{v}}1} & \cdots & \mathbf{m}_{\dot{\mathbf{v}}n} \\ \mathbf{m}_{\dot{\mathbf{w}}2} & \cdots & \mathbf{m}_{\dot{\mathbf{w}}n} \end{array}\right]$ denotes the nondiagonal inertia matrix, in which $\mathbf{m}_{\dot{\mathbf{v}}i}$ and $\mathbf{m}_{\dot{\mathbf{w}}i}$ are the inertia submatrices related to the accelerations of the ith limb and base-link linear and angular motions, respectively; $\mathbf{c}_{\mathbf{B}}\left(\mathbf{x},\dot{\mathbf{x}}\right)$ and $\mathbf{c}_{\mathbf{L}}\left(\mathbf{x},\dot{\mathbf{x}}\right)$ denote Coriolis and centrifugal force/torque vectors; $\mathbf{g}_{\mathbf{B}}\left(\mathbf{x}\right)$ and $\mathbf{g}_{\mathbf{L}}\left(\mathbf{x}\right)$ denote gravity force/torque vectors; $\tau_{\mathbf{L}}$ denotes generalized torque vector of limbs' joints; $\mathbf{J}$ denotes the Jacobian matrix; and $\mathbf{F}$ denotes external forces and moments acting on the robot, such as the reaction force of the floor.

Since a humanoid robot has a highly redundant mechanical structure, deriving Eq. (A.1) is not an easy task in general. A numerical algorithm can be used to systematically derive the closed form dynamic model of a humanoid robot as follows:

Inertia matrix:

1. Derivation of $\mathbf{m}_{\dot{\mathbf{v}}\dot{\mathbf{v}}}$, $\mathbf{m}_{\dot{\mathbf{w}}\dot{\mathbf{v}}}$ and $\mathbf{m}_{\dot{\mathbf{v}}i}$:

   for j = 1 : 3

$$\dot{\mathbf{x}} = \mathbf{0}; \ddot{\mathbf{x}} = \mathbf{0};\ \mathbf{g} = \mathbf{0}; \mathbf{F} = \mathbf{0}; \dot{\mathbf{v}}\left(j\right) = 1; \tag{A.2}$$

   for i = 1 : n

$$\left\{\left[{}^{i}\mathbf{f}_{\mathbf{B}}, {}^{i}\mathbf{n}_{\mathbf{B}}, {}^{i}\tau\right] = NE\left(i\right); \mathbf{m}_{\dot{\mathbf{v}}i}^{T}\left(j\right) = {}^{i}\tau\right\} \quad \text{end} \tag{A.3}$$

$$\hat{\mathbf{m}}_{\dot{\mathbf{v}}\dot{\mathbf{v}}}\left(j\right) = \sum_{i} {}^{i}\mathbf{f}_{\mathbf{B}};\ \ \mathbf{m}_{\dot{\mathbf{w}}\dot{\mathbf{v}}}\left(j\right) = \sum_{i} {}^{i}\mathbf{n}_{\mathbf{B}}; \dot{\mathbf{x}} = \mathbf{0}; \ddot{\mathbf{x}} = \mathbf{0};\ \mathbf{g} = \mathbf{0}; \mathbf{F} = \mathbf{0}; \dot{\mathbf{w}}\left(j\right) = 1; \tag{A.4}$$

   for i = 1 : n

$$\left\{\left[{}^{i}\mathbf{f}_{\mathbf{B}}, {}^{i}\mathbf{n}_{\mathbf{B}}, {}^{i}\tau\right] = NE\left(i\right); \mathbf{m}_{\dot{\mathbf{w}}i}^{T}\left(j\right) = {}^{i}\tau;\right\} \quad \text{end} \tag{A.5}$$

$$\mathbf{m}_{\dot{\mathbf{v}}\dot{\mathbf{w}}}\left(j\right) = \sum_{i} {}^{i}\mathbf{f}_{\mathbf{B}};\ \hat{\mathbf{m}}_{\dot{\mathbf{w}}\dot{\mathbf{w}}}\left(j\right) = \sum_{i} {}^{i}\mathbf{n}_{\mathbf{B}}; \tag{A.6}$$

   end

$$\mathbf{m}_{\dot{\mathbf{v}}\dot{\mathbf{v}}} = \hat{\mathbf{m}}_{\dot{\mathbf{v}}\dot{\mathbf{v}}} + m_B\mathbf{E_3};\ \ \mathbf{m}_{\dot{\mathbf{w}}\dot{\mathbf{w}}} = \hat{\mathbf{m}}_{\dot{\mathbf{w}}\dot{\mathbf{w}}} + \mathrm{I}_{\mathbf{B}}; \tag{A.7}$$

where n denotes the number of the limbs; $\mathbf{E_3}$ denotes a 3 × 3 identity matrix; $\mathbf{I_B}$ denotes the inertia of the base-link; and $NE()$ denotes the modified Newton–Euler algorithm in [34].

2. Derivation of $\mathbf{m}_{\dot{\mathbf{w}}i}, \mathbf{m}_{\dot{\mathbf{v}}i}$ and $\mathbf{m}_{ij}$:

for i = 1: n

$$\dot{\mathbf{x}} = \mathbf{0}; \ddot{\mathbf{x}} = \mathbf{0}; \mathbf{g} = \mathbf{0}; \mathbf{F} = \mathbf{0}; \tag{A.8}$$

for $j = 1 : i_k$

$$\left\{\ddot{\mathbf{x}}_{\mathbf{limb}} = \mathbf{0}; {}^{\mathbf{i}}\ddot{\mathbf{x}}_{\mathbf{limb}}(j) = 1; for\, k = 1 : n \left\{\left[{}^k\mathbf{f_B}, {}^k\mathbf{n_B}, {}^k\tau\right] = NE(k); \mathbf{m}_{ki}(j) = {}^k\tau;\right\} \quad end\right\} \tag{A.9}$$

$$\mathbf{m}_{\dot{\mathbf{v}}i}(j) = \sum_k {}^k\mathbf{f_B}; \quad \mathbf{m}_{\dot{\mathbf{w}}i}(j) = \sum_k {}^k\mathbf{n_B}; \tag{A.10}$$

end

end

Here, i_k denotes the degrees-of-freedom in the ith limb.

Hence, the inertia matrix is derived. The computational load can be decreased by using the symmetric property of the inertia matrix, i.e. $\mathbf{m}_{\dot{\mathbf{v}}\dot{\mathbf{w}}} = \mathbf{m}^T_{\dot{\mathbf{w}}\dot{\mathbf{v}}}$.

Coriolis and centrifugal vector:

$$\ddot{\mathbf{x}} = \mathbf{0}; \mathbf{g} = \mathbf{0}; \mathbf{F} = \mathbf{0}; \tag{A.11}$$

for $i = 1 : n \left\{\left[{}^i\mathbf{f_B}, {}^i\mathbf{n_B}, {}^i\tau\right] = NE(i)\right\}$ end

$$\mathbf{c_B}(\mathbf{x}, \dot{\mathbf{x}}) = \left[\sum_i {}^i\mathbf{f}^T_{\mathbf{B}}, \sum_i {}^i\mathbf{n}^T_{\mathbf{B}}\right]^T; \mathbf{c_L}(\mathbf{x}, \dot{\mathbf{x}}) = \left[\ {}^1\tau^T, \quad \cdots, \quad {}^n\tau^T\ \right]^T; \tag{A.12}$$

Gravity vector: The gravity vector is derived similarly by using Eqs. (A.11) and (A.12) and

$$\dot{\mathbf{x}} = \mathbf{0}; \ddot{\mathbf{x}} = \mathbf{0}; \mathbf{g} = \left[\ 0 \quad 0 \quad -9.8\ \right]^T; \mathbf{F} = \mathbf{0}; \tag{A.13}$$

Jacobian:

$$\dot{\mathbf{x}} = \mathbf{0}; \ddot{\mathbf{x}} = \mathbf{0}; \mathbf{g} = \mathbf{0}; \tag{A.14}$$

for j = 1 : 6 x p

$$\mathbf{F} = \mathbf{0}; \ \mathbf{F}(j) = 1; \tag{A.15}$$

$$\mathbf{F} = \mathbf{0}; \ \mathbf{F}(j) = 1; \tag{A.16}$$

for i = 1 : n

$$\left\{\left[{}^i\mathbf{f_B}, {}^i\mathbf{n_B}, {}^i\tau\right] = NE(i)\right\} \quad \text{end} \tag{A.17}$$

$$\mathbf{J}^T(j) = \left[\sum_i {}^i\mathbf{f}^T_{\mathbf{B}}, \sum_i {}^i\mathbf{n}^T_{\mathbf{B}}, \ {}^1\tau^T \quad \cdots \quad {}^n\tau^T\right]^T \tag{A.18}$$

end

Here, p denotes the number of forces acting on the robot.